3-D TRANSIENT SIMULATION OF AN AXYSIMMETRIC MICRO HEAT PIPE

Humberto Araujo Machado
Instituto de Aeronáutica e Espaço – IAE
Centro Técnico Aeroespacial - CTA
Pr. Mal. Eduardo Gomes, 50, Vila das Acácias
12228-904
São José dos Campos, SP
humbertoam@iae.cta.br

Faculdade de Tecnologia - FAT
Universidade do Estado do Rio de Janeiro – UERJ
Estrada Resende-Riachuelo s/n, Morada da Colina
27523-000
Resende, RJ
machado@fat.uerj.br

Abstract. *Micro heat pipes are formally defined as capillary heat pipes where the meniscus radius is smaller than the hydraulic radius. Such devices have been employed in electronic cooling, due its small dimensions and high heat exchange capacity, since this system provides excellent thermal control, assuring uniform temperature distribution. In previous works related to capillary heat pipe simulation, empirical or simple 1-D models have been used, but not taking into account the complete unsteady phenomena. In this work, the 3-D unsteady simulation of an axisymmetric micro heat pipe is presented, where the meniscus radius is considered constant along the transversal section. The phase change problem of a heated liquid meniscus in a groove is simulated via an interface tracking method, which is a hybrid Lagrangean-Eulerian method for moving boundary simulation, and has been adapted for use in irregular geometries*

Keywords*: Micro Heat Pipes, Interface Tracking Method, Moving Boundary, Phase Change.*

1. Introduction

The use of heat pipes in micro scale devices for cooling of electronic equipment has deserved attention, due its high heat transfer rates and excellent thermal control, improving the uniformity of temperature distribution, specially when built straight over the chips structure. As a consequence, micro heat pipes have been employed in high performance computers, laptops and workstations, satellites and space probes, fine surgery instruments, etc.

A Micro heat pipe (MHP) is formally defined as a capillary heat pipe where the meniscus radius is smaller then the hydraulic radius of the capillary grove it lies. The development of this kind of heat pipe has been done using empirical methods or simplified models. Most of the experimental works deal with a specific aspect of micro heat pipes, such as a particular shape or phenomenon involved in the pipe operation, or accuracy of any theoretical approximation used in the model. In these cases, some information is available about thermocappilary effects in a heated meniscus (Prat *et al*, 1998) or about the influence of geometry in the heat exchange process (Ravigururajan, 1998). In all experiments, several difficulties were found in reproducing the realistic dimensions and conditions of operation of a feasible M.H.P (Faghri, 1995). Huang et al (1998) studied a constrained vapor bubble behavior, and characterized it as a large version of a micro heat pipe. A strong dependence of its performance with the orientation with respect to gravity was observed.

Sun & Tien (1972) presented a simple conduction model for steady state operation with an enclosure condition, based in the local wall temperature and the mass flow rate, and compared with some experimental data available in literature. The results demonstrated the high heat transfer capacity of such devices, and its dependence to Biot number and relative contribution of radial conduction through the wick and axial conduction to the pipe wall.

Duncan and Peterson (1994) summarized the conclusions and limitations of each model available in an opened literature review. Krushtalev and Faghri (1994) have shown a one-dimensional model to predict the maximum heat exchange capacity and thermal resistance of a polygonal M.H.P, which was developed from some approximations based in empirical observations. Hopkins et al (1998) compared the one-dimension model to experimental data, obtained in test with trapezoidal micro heat pipes, in order to verify the maximum heat flux. Theoretical prediction of the capillary limitation in the horizontal orientation agreed reasonably with the experimental data.

Ma & Peterson (1998) investigated the minimum meniscus radius and the heat exchange limit in M.H.P through the conservation laws for momentum and Laplace-Young equation, providing analytical expressions for parameters of interest. Ha & Peterson (1998) have been developed a model where the differential expression is similar to Bernoulli's equation. An approximate analytical solution for the axial variation of meniscus curvature is presented. Peterson & Ma (1999) developed a more detailed model for a M.H.P through a 3rd order ordinary differential equation, that is able to

estimate the heat transport capacity and the temperature gradients along longitudinal coordinate, as a function of heat flux. However, all these works are 1-D models, just applicable to steady state processes.

The present work is an extension of the work presented by Machado (2002,2003,2004), where a mathematical model and a computational algorithm for simulation of the three-dimensional unsteady heat transfer and phase change processes in a square cavity, was proposed. In this work, the model is extended to irregular geometries, and a three-dimension section of an axesymmetric closed cavity is used to simulate the actual behavior of a micro heat pipe.

The phase change problem is solved via the interface tracking method proposed by Unverdi and Trygvason (1992), that is an hybrid Lagrangean-Eulerian method for moving boundaries, and has been employed to simulate fusion/solidification of crystals and metal alloys and bubble formation in nucleate boiling. This method has been successfully extended to three-dimensional problems of phase change (Esmaeeli & Arpaci, 1998; Shin & Juric, 2002) and bubble flow (Esmaeeli & Tryggvason, 1998, 1999; Arruda, 1999). Preliminary results show the behavior of the computer code for a simple case.

2. Physical problem and mathematical model

Consider a polygonal MHP having triangular corners (which can easily be extended for cross sections having different corner configurations), Fig.(1). The heat load is considered uniformly distributed between all corners. Taking advantage of the axesymmetry, the region for simulation can be limited to a half corner of a cross section. Consider such a cavity, filled with a pure Newtonian fluid with constant properties and isochoric behavior. Thermodynamic equilibrium is assumed in both phases, liquid and vapor, inside. The lateral and superior sides are considered thermally insulated.

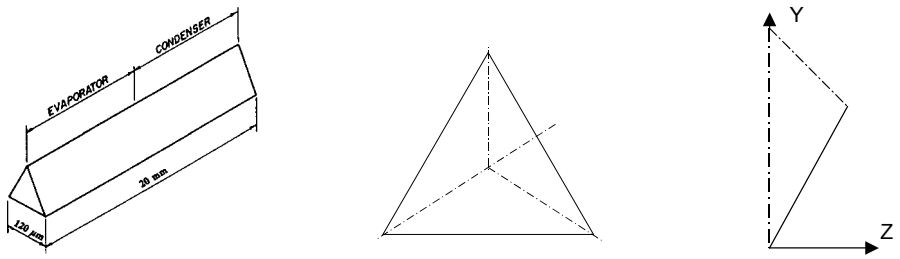

Figure 1. Axesymmetric MHP, cross-section and region of study.

The set of equations in dimensionless form used to represent the simple physical problem is written in an appropriate form to be solved by the interface tracking method, as proposed by Juric (1996). Terms in bold are vector quantities.

Continuity equation:

$$\frac{\partial \rho}{\partial t} + \nabla . \mathbf{w} = 0 \tag{1}$$

this form is equivalent to:

$$\nabla . \mathbf{w} = M \tag{2}$$

$$M = \int_A m \delta(\mathbf{x} - \mathbf{x_f}) dA \tag{3}$$

$$m = \left(\frac{\rho_v}{\rho_l} \right) \mathbf{V}.\mathbf{n} \tag{4}$$

where $\mathbf{w} = \rho \mathbf{u}$ (mass flux), $\mathbf{V}$ is the interface velocity, $\mathbf{n}$ is the interface normal vector, m is the mass flux through the interface per unit of area and $\delta(\mathbf{x} - \mathbf{x_f})$ is a 3-D delta function, that is non-zero only at the interface. Subscripts *l* and *v* refers to liquid and vapor phases, respectively. Tangential effects are neglected, as the fluid properties are assumed constant and uniform in each phase. Therefore, the interface velocity is supposed not having a tangential component.

Conservation of momentum:

$$\frac{\partial (\mathbf{w})}{\partial t} + \nabla . (\mathbf{w}\mathbf{u}) = -\nabla P + \frac{1}{Re} \nabla . \mu (\nabla \mathbf{u} + \nabla \mathbf{u}^T) + \mathbf{F} \tag{5}$$

where P is the pressure and $\mathbf{F}$ is a source term that takes into account the interfacial surface forces:

$$\mathbf{F} = \int_A \mathbf{f}\delta(\mathbf{x} - \mathbf{x_f})dA \tag{6}$$

where $\mathbf{x_f}$ is the interface position vector , $\mathbf{f}$ is the interface pressure due to the surface tension: $\mathbf{f} = (\kappa_I + \kappa_{II})$. $\mathbf{n}$/We, and κ is twice the mean curvature of the interface, and subscripts I and II are related to transversal and longitudinal directions, respectively.

Conservation of energy:

$$\frac{\partial(\rho cT)}{\partial t} + \nabla.(\mathbf{w}cT) = \frac{1}{Pe}\nabla.K\nabla T + Q \tag{7}$$

where c is the specific heat at constant pressure, K is the thermal conductivity and Q is a source term that takes into account the absorption or liberation of latent heat during phase change:

$$Q = \int_A q\delta(\mathbf{x} - \mathbf{x_f})dA \tag{8}$$

q is the source term of energy per unit of surface of the interface:

$$q = \frac{\rho_l L}{\rho_v L_0}(\rho\mathbf{V} - \mathbf{w}).\mathbf{n} \tag{9}$$

where L_0 is the latent heat of phase change and L is its corrected form, taking into account different specific heats for each phase:

$$L = L_0 + (c_l - c_v)T_v \tag{10}$$

The equations above, with the source terms included, satisfy the jump conditions automatically, assuming a thickless interface. Although specific volumes are different in the phases, the flow is assumed to be uncompressible, and both densities are considered constant. The total volume occupied for each phase remains constant during the heating. Therefore, the rates of condensation and evaporation must be the same, in order to satisfy the mass conservation within the cavity. During the transient process of heat transfer, the reference pressure inside the cavity rises and yields a correspondent increase of the local saturation temperature in every interface point, until the flow reaches steady state. The interface is supposed to be at thermal but not thermodynamic equilibrium (which supposes no temperature jump at the interface). This hypothesis added to the Clausius-Clapeyron relation applied to a curved surface, but neglecting the kinect mobility effects yields the temperature condition at the interface as a function of the reference pressure:

$$T_f - T_{SAT} - \sigma\kappa + We.T_{SAT}\left(1 - \frac{\rho_l}{\rho_v}\right)(P_f - P_\infty) + \frac{\rho_v}{\rho_l}\left(\frac{c_v}{c_l} - 1\right)(T_f - T_{SAT})^2 + \vartheta(\rho\mathbf{V} - \mathbf{w}).\mathbf{n} = 0 \tag{11}$$

where T_f is the local interface temperature, T_{SAT} is the local saturation temperature (from the equation of state), P_f is the local interface pressure, P_{oo} is the reference pressure within the cavity, $\sigma = c_l T_o\gamma/\rho_v L_o^2 y_o$. T_o is the reference temperature, y_o is the reference length and γ is the surface tension. Last term includes the non-equilibrium effects in the molecular kinetics: $\vartheta = \rho_l c_l U_0 / \rho_v L_0 \varphi$, where φ is the molecular kinetics coefficient. Small values of φ suppress the growth of protrusions in the interface. The non-dimensional numbers resulting from the mathematical model are: Reynolds number, $Re = \rho_l U_0 \lambda/\mu_l$, Peclet number, Pe = Re.Pr, Weber number, $We = \rho_l U_0^2 \lambda/\gamma$ and Froude number, $Fr = U_0^2/G.y_0$ (G is the local acceleration of gravity).

3. Method of solution

The moving boundary problem was solved by the Interface Tracking Method, introduced by Unverdi & Trygvason (1992), and employed by Juric (1996) in the solution of phase change problems. In this method, a fixed uniform Eulerian grid is generated, where the conservation laws are applied over the complete domain. The interface acts as a Lagragean referential, where a moving grid is applied. The instantaneous placement of the interface occurs through the constant remeshing of the moving grid, and each phase is characterized by the Indicator Function, represented by I($\mathbf{x}$,t), which identifies the properties of vapor and liquid phases.

The interface surface is built considering the transversal radius (R_I) constant (according to the formal definition of a micro heat pipe), and its longitudinal shape is represented as a parametric curve, $\mathbf{R}$(u), where the normal and tangent vectors, longitudinal radius (R_{II}) and curvature are extracted from. The interface discretization is shown in Fig (2). The osítions of interface points in transversal direction are interpolated by a Lagrange polynomial, which allows to obtain

the geometric parameters and remeshes the curve, keeping the distance *d* between curve points within the interval 0.9 < d/h < 1.1, where *h* is the distance among the fixed grid points, as shown in Fig. (2).

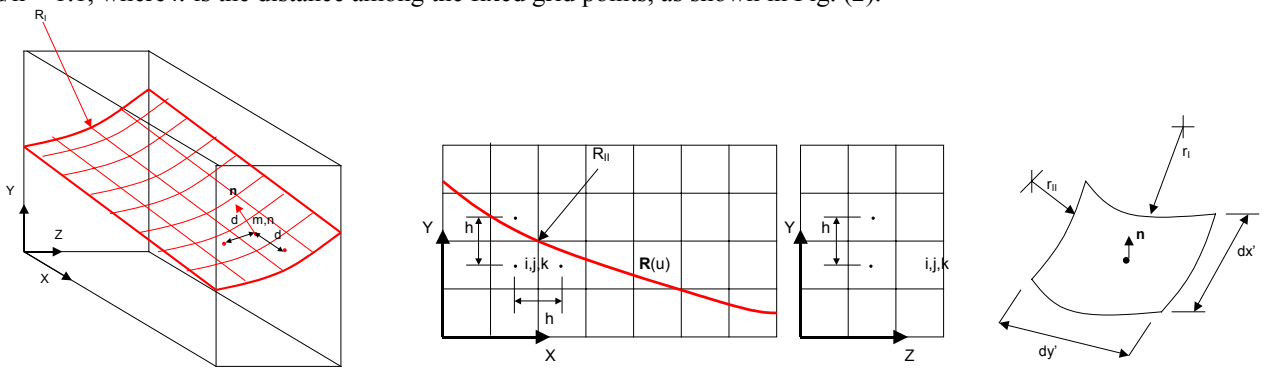

Figure 2. Interface discretization – Lagrangean mesh and surface element, dS.

The number of interface points in z-direction is controlled by the interface arc inside the domain, Fig. (3). In order to built the Eulerian mesh, the domain's borders (wall and symmetry lines) are use to limit a regular grid, where each grid element is a square. Such representation improves as more points are added to the mesh.

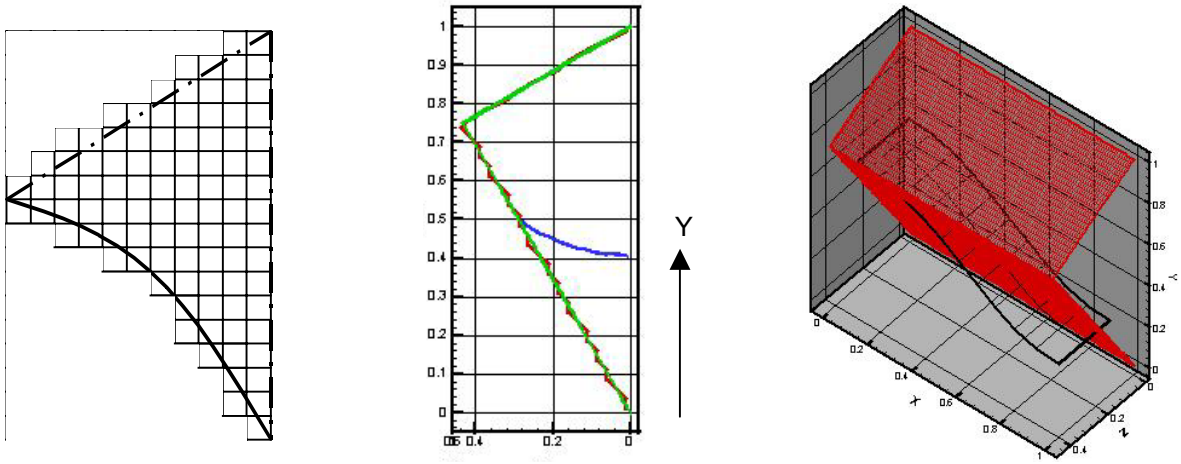

Figure 3. Eulerian mesh; exact domain's (green), mesh limits for 50 point in y-direction (red), interface (blue); 3-D view.

The Indicator Function varies from 1 (vapor) to 0 (liquid), and is numerically constructed using the interface curve to determine a source term **G(x)**. The jump across the interface is distributed over the fixed grid points, yielding a gradient field in the mesh:

$$\mathbf{G(x)} = \nabla I = \int_A \mathbf{n}\delta(\mathbf{x} - \mathbf{x_f})dA \tag{12}$$

which should be zero, except over the interface, as represented by the Dirac Delta Function. However, such representation is not convenient for a discrete number of points. The Distribution Function is used to represent the interface jump. Such Function is a curve similar to a Gaussian one, and its value depends on the distance $|\mathbf{x}_{ij} - \mathbf{x}_k|$ among the Lagrangean and Eulerian points:

$$D_{i,j,k}(\mathbf{x}_{m,n}) = \frac{f[(x_{m,n} - x_i)/h].f[(y_{m,n} - y_j)/h].f[(z_{m,n} - z_k)/h]}{h^3} \tag{13}$$

where D_{ij} is the Distribution Function for a point *k* in the Lagrangian mesh in relation to a Eulerian point and the function *f* is a probability distribution (Juric, 1996). One should note that increasing h, the interface becomes thicker.

The vector **G(x)** is obtained from:

$$\mathbf{G_{i,j,k}} = \sum_{m,n} D_{i,j,k}(\mathbf{x_{m,n}}).\mathbf{n}(\mathbf{x_{m,n}}).dS(\mathbf{x_{m,n}}) \tag{15}$$

where $dS(x_{m,n})$ is the surface element, shown in Fig. (2), and given as $dS = dx'.dy'$.

The divergence of the gradient field is found by numerical derivation of Poison's equation:

$$\nabla^2 I = \nabla.\mathbf{G} \tag{16}$$

Despite of being considered constants in each phase, the properties inside the domain must be treated as variable in the formulation. A generic property ϕ (ρ, μ, c ou K) is expressed as:

$$\phi(\mathbf{x}) = \phi_l + (\phi_v - \phi_l)\, I(\mathbf{x},t) \tag{17}$$

The coupling between the moving mesh and the fixed grid is done at each time step, through the Distribution Function, that represents the source terms in the balance equations and interpolates the fields with infinitesimal discontinuities into a finite thick region at the interface.

The initial interface shape is first specified and then the Indicator Function is constructed. The property and temperature fields are determined. The iterative process targets the reference pressure and its correspondent interface velocity at each time step. The steps to be followed are:

1. Using the current value of **V**, the interface points are transported to a new position, calculated explicitly through the equation $\mathbf{V}^n = (d\mathbf{x}_f/dt).\mathbf{n}$;
2. Density and specific heat are calculated at the new interface position;
3. Surface tension **f** is calculated and distributed into the fixed grid;
4. In the first iteration, reference pressure is estimated, and after it is corrected according to the mass flux residual.
5. $\mathbf{V}^{n+1}$ is estimated via Newton iterations, using a numerical relaxation schedule, and used to calculate the mass flux m crossing the interface. The interface mass flux is distributed in the fixed gird;
6. According to boundary conditions, **w**, **u** e P are obtained from Eqs. (2) and (5);
7. Density found in step 2 and flux **w** are interpolated via distribution function in order to find the mass flux $\mathbf{w}_f$ and density ρ_f at the interface;
8. Heat flux q is calculated through Eq. (9) and distributed into the fixed grid;
9. According to boundary conditions, energy equation - Eq. (7) is used to obtain the temperature at time n+1;
10. Temperature and pressure are interpolated to find T_f and P_f at the interface;
11. The equilibrium condition is tested. If it is not satisfied, a new estimate for $\mathbf{V}^{n+1}$ is calculated and returns to step 5.
12. The mass flux residual is calculated, and if it is lower than the reached tolerance, the fields of viscosity and conductivity are updated for the new position, advance one step time, otherwise returns to step 4.

The convergence criterion used in step 11 is the residual in Eq. (11). Once it has reached the desired tolerance, convergence for interface velocity is assumed. Otherwise, the velocity is corrected via Newton Iterations, given as:

$$\mathbf{V}^{n+1} = \mathbf{V}^n - \omega.R(T) \tag{18}$$

where ω is a constant and R(T) is the residual for the temperature jump condition at the interface. Iteration are repeated until R(T) in every point become smaller than the tolerance. The optimum value for ω is found by tentative, at the beginning of the calculation. A similar schedule is used to obtain the reference pressure, where the mass flux residual is the algebraic summation of the source term M, Eq. (3), along the interface.

4. Results

Preliminary results for 3-D unsteady simulation were obtained for a square cavity with triangular transversal section representing a micro heat pipe, considering the effects surface tension. Gravity effects were neglected, in order to take advantage of the axesymmetry. The domain considered is the region defined as $0 < x < 1$ and $0 < y < 1$ and limited by the symmetry axe and triangle sides, under prescribed temperatures in the walls, $T_w = 11$, in $0 < x < 0.25$ and $T_w = -9$, in $0.75 < x < 1.0$, considering $T_0 = 1$ the dimensionless saturation temperature as the initial condition. In the intermediary section, $0.25 < x < 0.75$, the wall is thermally insulated, $q_w = 0$. The values used in the test case, for the physical parameters, were: $K_v/K_l = 0.5$, $\rho_v/\rho_l = 0{,}9$ $c_v/c_l = 0.5$, $\mu_v/\mu_l = 0.5$, Pe = 2, Re= 1, We = 3.96, Fr = 3.92, $\sigma = 0.99$ e $\vartheta = 0.4$, and the interface is placed at $y = 0.5$ at $t = 0$. A 10 x 10 points grid was used in x and y direction. The schedule for correcting the reference pressure was tested using a simplified second order polynomial as the equation of state, given as $T_{SAT} = 0.1.(P+P_{oo})^2 + T_{v0}$, where T_{v0} is the saturation temperature for the initial reference pressure, equal to 1. For this case, the initial value for the reference pressure is taken to zero.

Figure (4) shows the variation of the reference pressure along the time for different values of the meniscus radius. Reference pressure varies strongly with the radius. When R = 2, steady state is not reached before the interface touch

the superior wall (when the calculation stops). The curve for R = 10^{10} (infinite) reaches steady state faster. In Fig. (5), the evolution of interface position with the time (starting as a horizontal line) is shown for R infinite, demonstrating the good behavior of the grid reconstruction schedule. Interface shape when steady state has been reached, Fig. (6), presents little variation, although a small displacement of the center of circulation can be observed.

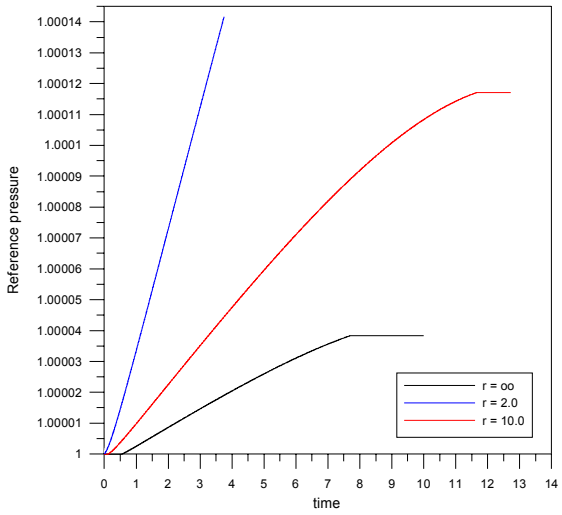

Figure 4. Reference pressure variation with time.

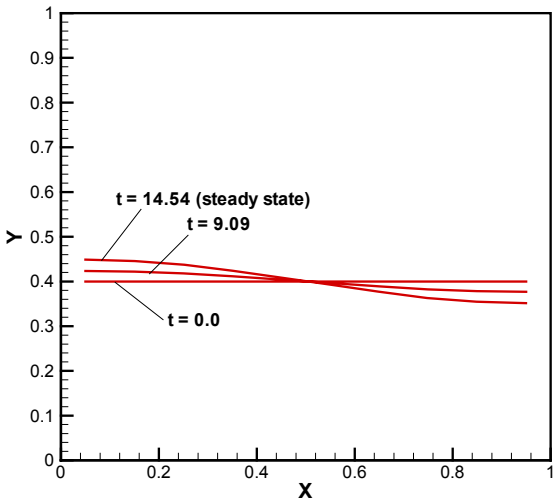

Figure 5. Interface shape evoltuion for R infinite.

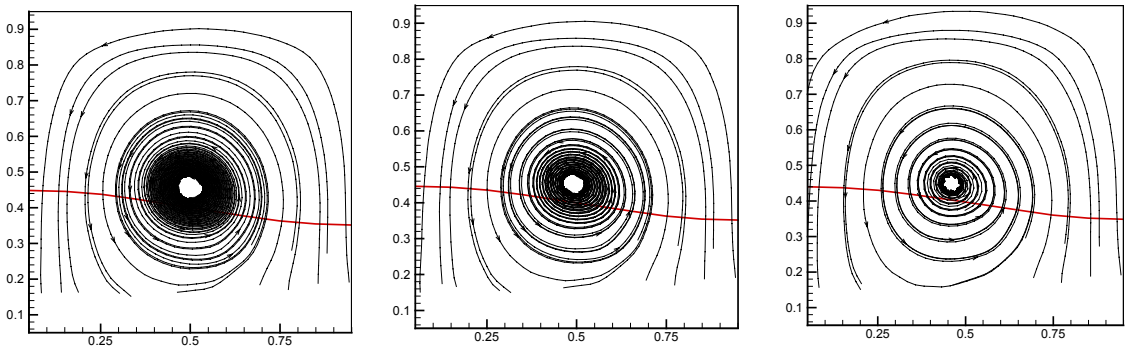

a) R infinite b) R = 10 c) R =2, t= 12.5

Figure 6. Streamlines in z = 0.5.

. Figure (7) shows the transversal velocity profile at x = 0.5 for R infinite. Symmetry is this cross section is straight observed, since there is no flux across the right and superior edges (symmetry lines), Fig. (7.a). A tendency of recirculation can be observed in velocity field, Fig. (7.b,c), what should be more visible with the use of a refined grid.

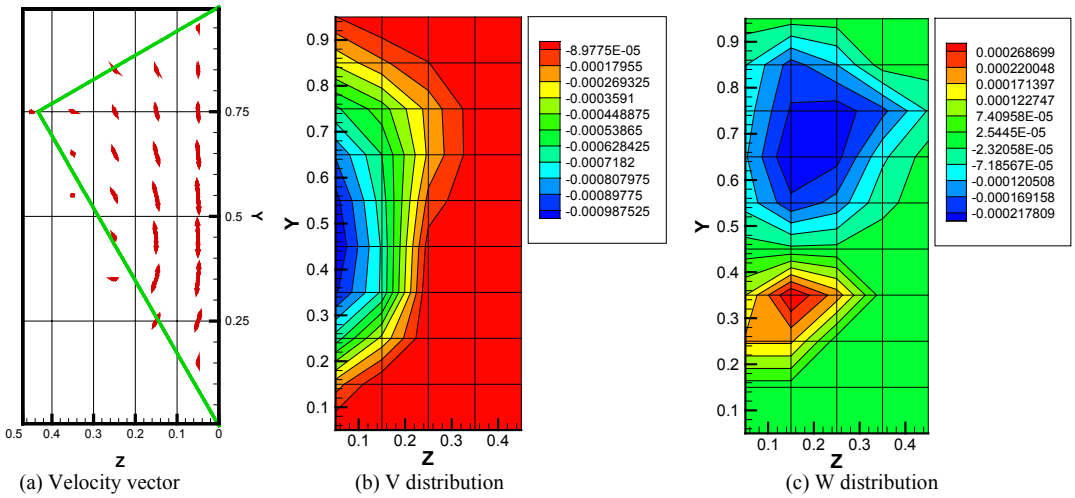

(a) Velocity vector (b) V distribution (c) W distribution

Figure 7. Velocity distribution in x = 0.25 for R infinite, at steady state.

In Fig. (8), interface temperature and pressure over the interface surface are shown. Interface temperature varies according to the jumping conditions, from Eq. (12). Variation of pressure is influenced by the increase of the longitudinal radius of curvature of the meniscus.

Table (1) shows the values for dimensionless thermal resistance that decreases with meniscus radius. It is in opposition to the behavior reported by Machado (2003) for a flat square heat pipe under same conditions. The main difference is related to geometry: the surface submitted to the difference of temperature is quite greater in this case and is also in contact with the vapor phase, while in the previous work only liquid phase was in contact to the boundary temperatures, in the heat pipe's basement.

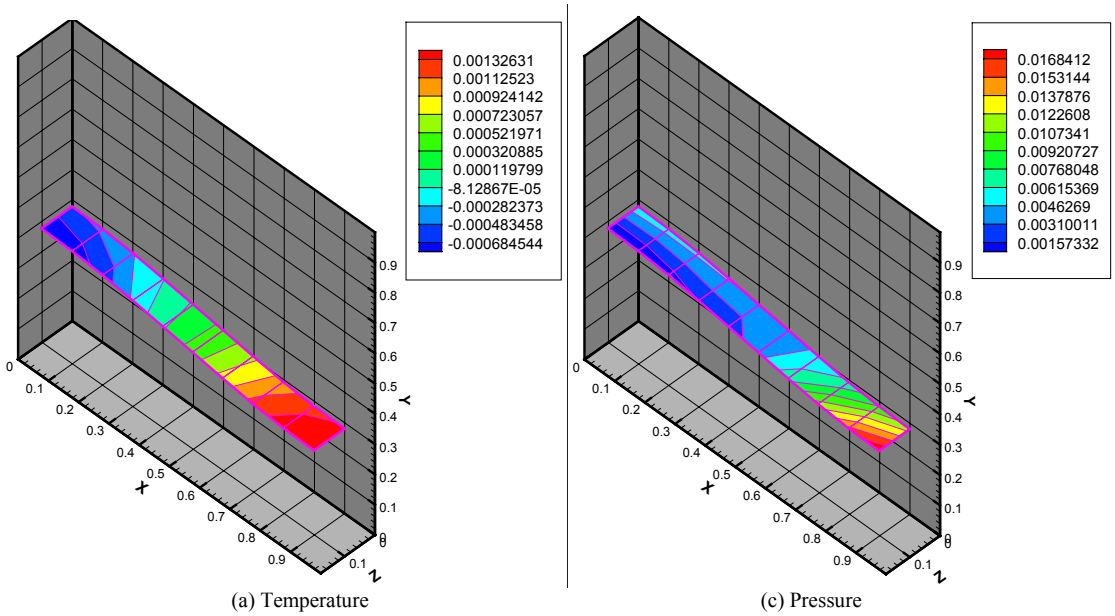

(a) Temperature (c) Pressure

Figure 8. Interface velocity, temperature and pressure for R = infinite at steady state.

Table 1. Dimensionless thermal resistance as a function of transversal meniscus radius.

Radius	Thermal resistance	obs
Infinite	8.009059229963809E-001	Steady state
10.0	7.542673108128405E-001	Steady state
Infinite	1.064544627588111	t = 3.1
10.d0	1.046721375870734	t = 3.1
2.0	1.043136871950504	t = 3.1
1.5	1.043049551336578	t = 3.1
1.2	1.042926248430496	t = 3.1
1.0	1.042768906977973	t = 3.1
0.8	1.042475033085603	t = 3.1

5. Conclusions

In this work, the Interface Tracking Method was employed to simulate the unsteady 3-D heat transfer and phase change process inside an axesymmetric capillary heat pipe, represented by a square closed cavity with triangular cross-section. A regular mesh constructed with square elements represented the non-retangular geometry. The number of such elements varies according to the distance of the edge from the symmetry line. Such representation improves as more points are added to the Lagrangean mesh.

The complete physical model was tested, considering a constant transversal meniscus radius, and the method shown to be able to represent the physical process end capture the differences due to the variation of the transversal meniscus radius. The radius rising yields a delay in reaching the steady state, decreases thermal resistance and increases reference pressure, with an opposite behavior when compared with previous works concerned to rectangular heat pipes under same conditions.

Although a rough mesh was employed, the results present physical coherence and are qualitativelly close to that expected for a heat pipe. Complete test for fluids and dimensions found in feasible heat pipes in refined meshes are necessary for comparison to the one-dimensional models and experimental data available in literature, in order to verify the accuracy of the physical model. The methodology described in this work can be easily extended to any kind of irregular geometries.

6. Acknowledgements

The author would like to acknowledge to FAPESP - the scientific sponsor agency of the Brazilian State of São Paulo - for the financial support during this work.

7. References

Arruda, J. M., 1999, Simulação Numérica dos Processos de transporte, Deformação e Captura de Interfaces tridimensionais, Msc. Thesys, Universidade Federal de Uberlândia.

Cotta, R. M., 1998, The Integral Transform Method in Thermal and Fluids Science and Engineering, Begell House, New York.

Duncan, A. B., Peterson, G. P., 1994, Review of Microscale Heat Transfer, Applied Mechanics Review, v. 47, n. 9, pp. 397-428.

Esmaeeli, A., Arpaci, V., 1998, Numerical Modeling of Three-dimensional Fluid Flow with Phase Change, Proc. 4th Microgravity Fluid Physics & Transport Phenomena Conference, Cleveland, Ohio, pp. 546-551.

Esmaeeli, A., Tryggvason, G., 1998, Direct Numerical simulation of Bubble Flows - Part 1 – Low Reynolds Number Arrays, J. Fluid Mechanics, v. 377, pp. 313-345.

Esmaeeli, A., Tryggvason, G., 1999, Direct Numerical simulation of Bubble Flows - Part 2 – Moderate Reynolds Number Arrays, J. Fluid Mechanics, v. 385, pp. 325-358.

Faghri, A., 1995, Heat Pipe Science and Technology, Taylor&Francis, NY.

Hopkins, R., Faghri, A., Khrustalev, D., 1999, Flat Miniature Heat Pipes with Micro Capillary Grooves, J. Heat Transfer, v. 121, pp. 102-109.

Huang, J., Karthikeyan, M., Plawsky, J., Wayner Jr., P.C., 1998, Constrained Vapor Bubble, Proc. 4th Microgravity Fluid Physics & Transport Phenomena Conference, Cleveland, Ohio, pp. 155-159.

Juric, D., 1996, Computations of Phase Change, PhD. Thesis, University of Michigan.

Juric, D. and Tryggvason, G., 1998, Computations of Boiling flows, Int. J. of Multiphase flow, vol. 24, no. 3, pp 387-410.

Khruhstalev, D., Faghri, A., 1994, Thermal Analysis of a Micro Heat Pipe, Journal of Heat Transfer, v. 116, pp. 189-198.

Ma, H. B., Peterson, G. P., 1998, The Minimum Meniscus Radius and Capillary Heat Transport Limit in Micro Heat Pipes, Journal Heat Transfer, v. 120, pp. 227-233.

Machado, H. A., Miranda, R. F., 2001, Simulation of Micro Heat Pipes Using an Interface Tracking Method, Proceedings of the XVI COBEM - Brazilian Congress of Mechanical Engineering, Uberlândia, Brazil.

Machado, H. A., 2003, Simulation of a Flat Capillary Heat Pipe Using an Interface Tracking Method, Proceedings of the XVII COBEM - Brazilian Congress of Mechanical Engineering, São Paulo, Brazil.

Machado, H. A., 2004, 3-d Transient Simulation of a Flat Capillary Heat Pipe Via an Interface Tracking Method, Proceedings of the X ENCIT - Brazilian Congress of Thermal Sciences and Engineering, Rio de Janeiro, Brazil.

Peterson, G. P., 1994, "An Introduction to Heat Pipes – Modeling, Testing and Applications", John Wiley & Sons, New York..

Peterson, G. P., Ha, J. M., 1998, Capillary Performance of Evaporating Flow in Micro Grooves: An Approximate analytical Approach and Experimental Investigation, Journal Heat Transfer, v. 120, pp. 743-751.

Peterson, G. P., Ma, H. B., 1999, Temperature Response of Heat Transport in a Micro Heat Pipe, Journal Heat Transfer, v. 121, pp. 438-445.

Prat, D. M., Brown, J. R., Hallinan, K. P., 1998, Thermocapillary Effects on the Stability of a Heated, Curved Meniscus, Journal Heat Transfer, v. 120, pp. 220-226.

Ravigururajan, T. S., 1998, Impact of Channel Geometry on Two-Phase Flow Heat Transfer Characteristics of Refrigerants in Microchannel Heat Exchangers, Journal Heat Transfer, v. 120, pp. 485-491.

Shin, S., Juric, D., 2002, Modeling three-dimensional Multiphase flow Using a Level contour Reconstruction Method for Front Tracking Without Connectivity, J. Comp. Physics, v. 180, pp. 427-470.

Sun, K. H., Tien, C. L., 1972, Single Conduction Model for Theoretical Steady-State Heat Pipe Performance, AIAA Journal, v. 10, pp. 1051-1057.

Unverdi, S. O., Tryggvason, G., 1992, A Front-Tracking Method for Viscous, Incompressible, Multi-fluid Flows, Journal of Computational Physics, v. 100, pp. 25-37.